Laser Engraving Processes on AISI 304 Stainless Steel: A Multi-Objective Optimization Approach

A. S. Abegunde [a*], O. O. Ojo [b], P. K. Farayibi [b] and A.M Adeyinka [c]

[a] *Department of Mechanical Engineering, Federal University of Technology, Akure, Nigeria.*
[b] *Department of Industrial and Production Engineering, Federal University of Technology, Akure, Nigeria.*
[c] *Department of Mechanical Engineering, Auburn University AL 36842, USA.*

Authors' contributions

This work was carried out in collaboration among all authors. All authors read and approved the final manuscript.

Original Research Article

ABSTRACT

Laser engraving is becoming a preferred alternative to conventional machining for industrial post-processing due to its higher accuracy and elimination of tooling challenges. It is widely used for creating precise engravings on components in industries such as aeronautics, medical devices, printing, and general aesthetic applications. This research is developed around AISI 304 stainless steel based on its versatile use in various applications, investigating the influence of key laser engraving processing parameters such as laser power, scan speed, exposure time, and number of passes on output characteristics such as surface roughness, kerf width, engraving depth, and material removal rate. Analysis of variance and main effect plots were used to determine the

_____

Corresponding author: Email: abegundesademola@gmail.com;

optimal parameters for individual response while multi-response optimization to obtain a unified parametric combination was done by combining principal component analysis with a grey relational approach. The best combination of these processing parameters obtained for the multi-response optimization is (1, 0, 0, -1) which implies 15 W laser power, 28.57 mm/s scan speed, exposure time of 20 ms and (1) no of pass. The study has been able to establish that integration of grey relational analysis and principal component analysis shows a robust approach in investigating multi-objective optimization of processes.

Keywords: Laser engraving; AISI 304 stainless steel; multi-objective optimization; principal component analysis; grey relational approach.

ABBREVIATIONS

AISI	*: American Iron and Steel Institute*
SS	*: Stainless Steel*
RSM	*: Response Surface Methodology*
DOE	*: Design of Experiment*
SPM	*: Scanning Probe Microscope*
PCA	*: Principal Component Analysis*
GRA	*: Grey Relational Analysis*
GRC	*: Grey Relational Coefficient*
GRG	*: Grey Relational Grade*
SR	*: Surface Roughness*
KW	*: Kerf Width*
ED	*: Engraving Depth*
MRR	*: Material Removal Rate*
ANOVA	*: Analysis of Variance*

1. INTRODUCTION

Laser engraving process is a non-conventional machining process that uses thermal energy in the removal of material from the workpiece surface (Sugar et al. 2013, Patel et al. 2022). It has been established as an alternative to conventional methods of material removal in a wide range of industrial applications (Knowles et al. 2007, Ahmed et al. 2016). The material removal process takes place by sublimation, which occurs as a result of the laser-material interaction leading to atomic vibration of the material to generate sufficient heat for sublimation to occur (Brown and Arnold 2010, Stavropoulos et al. 2012). Laser, being an intense source of electromagnetic radiation is highly monochromatic and coherent, wherein the high-power laser density is released within a short time interval (pulse duration) onto a target spot that is a few micrometers in diameter and can reliably produce high-resolution patterns onto various metal such as copper and stainless steel (Brousseau et al. 2010). In industries, engraving, selective ablation and machining of different materials are made possible with the introduction of laser sources characterized by short and ultra-short pulses having from nanosecond to femtosecond duration (Stavropouloset al. 2012). Engraving processes are performed on a product surface for the purpose of product identification, traceability (Daniel 2000) and surface cleaning for high dimensional accuracy (Arnold 2002).

Engraving is further employed in printing processing where engraved plates are used as a mold for different patterns in the industrial production of security printings (e.g., banknotes, passports and visas), the desired pattern (e.g., micro letters, lines and images) can be achieved by laser ablation (Haron and Romlay 2019). Over the years, micromachining has been employed as conventional means of achieving engraving on various component parts however, the procedure is slower and requires tooling, jigs, and fixtures. These setbacks are being overcome by laser engraving as it can rapidly achieve the same or more precise output with faster turnaround time, without tooling, and a high degree of automation. However, the degree of precision of shape, the removal rate and the surface quality typical of the engraving process strictly depend on the material's properties, the laser source characteristics and the process parameters (Hubeatir 2018). To achieve any

desired output characteristics or responses on engraved surfaces, process optimization is required.

Over the past decades, several experiments involving laser-beam engraving have been reported by researches, discussing different processing conditions and surface integrity of ablated surfaces (Hribar et al. 2022). (Campanelli et al., 2007) used the design of experiments to analyze the effect of process parameters (scan speed, frequency, power, overlapping and scan strategy) on the surface roughness and the depth of removed material. (Saklakoglu and Kasman 2011) investigated the influences of the laser-engraving process parameters on the surface roughness and the groove depth, using AISI H13 hot-working steel and a 30 W fibre laser source. Regression analysis was used to model the effect of the process parameters on surface roughness and the groove depth, their result showed that the 20kHz pulse frequency, 18W laser power and 800 mm/s scan speed produced the lowest surface roughness while the maximum groove depth was achieved at the maximum pulse frequency of 40 kHz. (Mladenovic et al., 2016). studied laser engraving of AISI 304 stainless steel using Response-Surface Methodology, where it was reported that the removal rate, the groove depth and the groove width at zero plane are highly influenced by the scan speed. (Angshuman et al., 2018) investigated the effect of process parameters such as laser power, scanning speed and pulse frequency of laser beam on marking width and marking depth using response surface methodology (RSM). Their result showed that maximum mark width and mark depth can be obtained at a laser power of 6.96 W, pulse frequency of 16.69kHz and scanning speed of 6.60 mm/s. (Patel and Patel 2014) have conducted a review on the parametric optimization of laser engraving process for different materials using grey relational technique. They considered the effect of different input parameter such as spot diameter, laser power, laser frequency and wavelength on output parameters like material removal rate, surface finish and indentation. (Mathias et al., 2023) investigated the impact of laser scanning patterns on Laser Surface Melting (LSM) with 316L stainless steel. The commonly used Cartesian "zigzag" pattern with a radial pattern was compared, evaluating their effects on the material's properties. The study revealed that varying the scanning pattern significantly altered the stress state and deformation of the

specimens. Key outcomes included increased crystallite size, reduced dislocation density, slight hardening of the melted layer, and decreased toughness. These findings highlight the importance of scanning patterns in optimizing LSM processes for improved material performance. (Yue et al., 2024) also established that laser transformation hardening process has shown to enhance yield strength, ultimate tensile strength and elongation in processed material. Microstructural changes, including refined grain size and increased martensite content, were linked to improved strength and ductility. However, excessive laser power led to grain growth due to longer cooling times.

In conclusion, several research works have been conducted on surface optimization of the process parameters affecting the quality of the ablated surface where in some cases the focus has been on single optimization of selected responses. However, the optimization of just one output characteristics may not necessarily be the best for another output characteristic. Hence, this study extensively investigates the relationship of selected process parameters on several responses and multi-objective optimization of selected responses by combining principal component analysis with the grey relational approach.

2. METHODOLOGY

2.1 Materials

AISI 304 stainless steel material of 1mm thickness was sourced and used as the engraving material for this work. AISI 304 is an austenitic stainless steel known for delivering greater corrosion and heat resistance, high ductility, excellent drawing, forming, and spinning properties. Table 1 shows the chemical composition of the AISI 304 SS respectively.

A 15W fiber laser engraving machine was designed and developed for this work due to its short wavelength (ζ = 450 nm) making it ideal for cutting reflective metal materials, as shown in Fig. 1.

The stainless-steel surfaces were grit blasted to improve laser absorptivity and cleaned with acetone to remove contaminants prior to the laser processing. During the experiments, the laser beam is focused onto the workpiece surface at a 20 mm focal length which yields a beam spot diameter of 0.15 mm. The motion of

the laser beams and the process parameters is controlled by the laser engraving software. The laser output power was set at three distinct levels and four factors. Table 2 presents the parameters, and the levels employed in engraving of the stainless steel specimen.

2.1.1 Measurement of engraved characteristics

A 27 experimental run was obtained and conducted based on the box-Behnken design of experiment (DOE) given four factors at three levels. Each SS specimen was engraved by an 8.5mm x 2.3 mm area. The following geometrical response variables were investigated: surface roughness, groove depth (h_g) and kerf width at zero plane (w_o) and material removal rate which is a function of the engraved area (A_g) against the time taken, as shown in Fig. 2.

AA3000 Scanning Probe Microscope (SPM) shown in Fig. 3 was used to obtain surface data of the required output responses from the engraved area of the processed samples. The measurement was made at three distinct locations from the engraved specimen surface and the mean of each response was recorded.

Table 1. The chemical composition of AISI 304 SS

C	Cr	Mn	Ni	Si	S	P	N	Fe
0.04%	18.11%	1.28%	8.02%	0.35%	0.01%	0.03%	0.05%	Bal
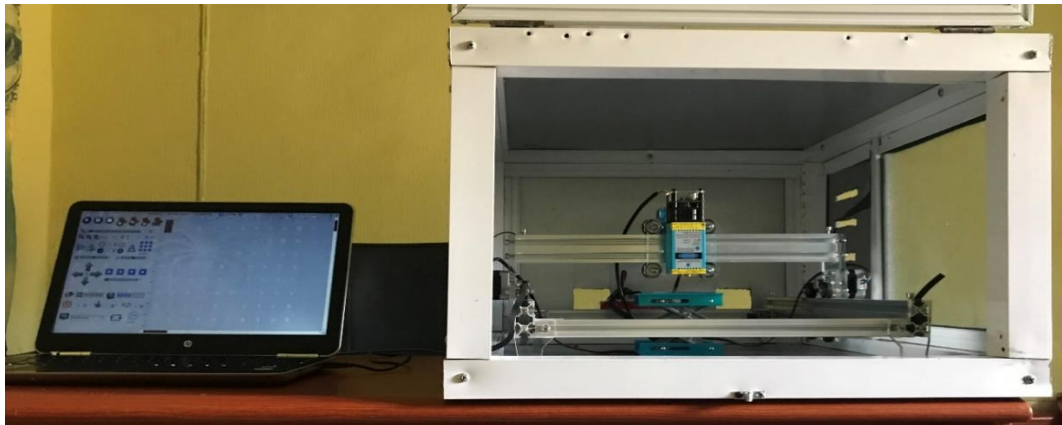
Fig. 1. The experimental setup

Table 2. Laser engraving parameters and their levels

Engraving parameter (factor)	low (-1)	medium (0)	high (1)
Power, P (W)	11	13	15
Scan speed, (mm/s)	21.43	28.57	35.72
Exposure Time (ms)	15	20	25
No of passes	1	2	3
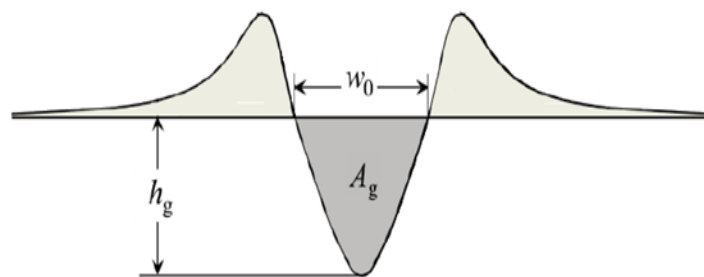
Fig. 2. A schematic of the cross-sectional profile of a laser engraved groove (Mladenovič et al. 2016)

Fig. 3. SPM AA 3000

2.1.2 Output characteristics and data analysis

Surface roughness responses, kerf width, engraving depth, and material removal rates are responses needed to be obtained. These output characteristics were obtained by taking surface profilometry of the specimens on AA3000 Scanning probe microscope Imager. Fig. 4 (a) and (b) shows a sample of the engraved area as view by AA3000 SPM from one of the specimens.

The measurements were carried out three times average from SPM Imager as seen in Fig. 5 and Fig. 6 below and the mean values of each response were recorded and reported.

2.2 Methods

2.2.1 Multi-objective optimization approach

The multi-objective optimization was achieved using the Box-Behnken Design (BBD) combined with Grey Relational Analysis (GRA) and Principal Component Analysis (PCA). The process began by selecting the Box-Behnken Design to determine the experimental runs and process factor combinations. Grey Relational Coefficients (GRC) were then calculated from the experimental responses. PCA was applied to the GRC to determine the weighting values, which were used to calculate the Grey Relational Grade (GRG). The GRG was used for plotting the main effects and performing analysis of variance to identify the optimal parameters for the engraving process. Minitab software was utilized for the analysis,

Box-Behnken design of experiment was used to achieve a 27 orthogonal array based on Table 2 and the corresponding experiment run is presented in Table 3. These arrays were the basis in which the process factor combinations used for the experiment were subjected.
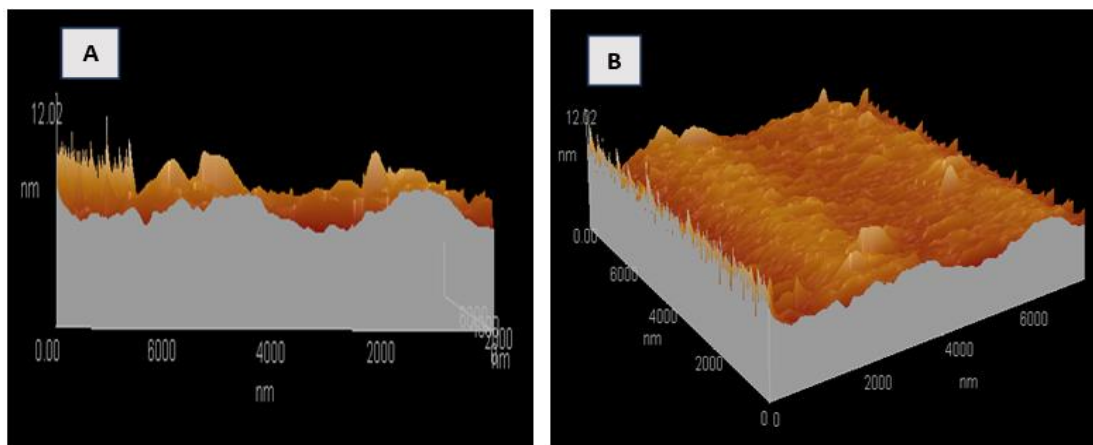

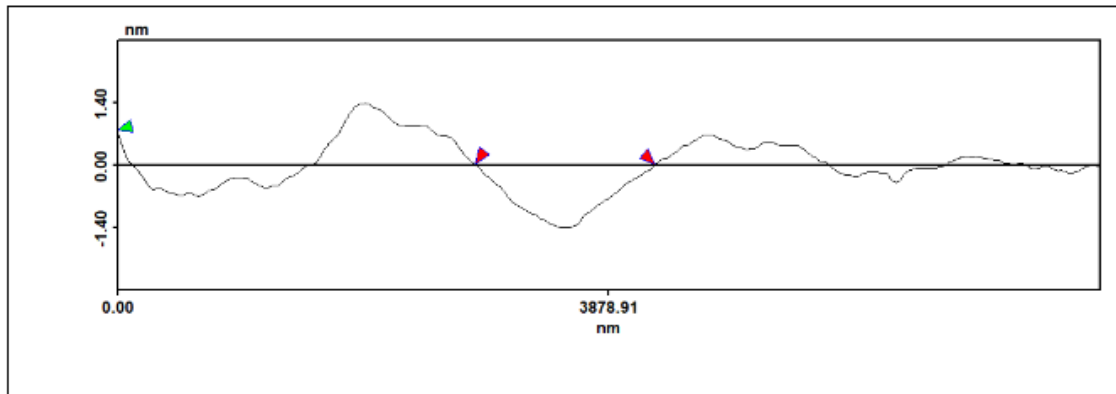**Fig. 4. Engraved area (a) 3D side view (b) 3D Isometric side view**

Surface distance:1415.49nm
Horizontal distance:1415.49nm   Vertical distance:0.01nm
Angle(degree):-0.00   Roughness Ra:0.374 nm
Height[Red]:6.03nm   Height[Greeb]:6.04nm
Size:8000.0(nm)*8000.0(nm)   Image Height:12.02(nm)

Fig. 5. Imager showing kerf width Section

Table 3. Orthogonal array for the experiment

No	Process Parameter			
	A (W)	B (mm/s)	C (ms)	D
1	15	28.57	20	3
2	13	21.43	25	2
3	13	28.57	15	1
4	13	28.57	20	2
5	11	28.57	25	2
6	13	35.72	20	1
7	13	35.72	25	2
8	13	21.43	20	1
9	11	28.57	20	3
10	13	21.43	20	3
11	15	28.57	15	2
12	11	35.72	20	2
13	15	28.57	25	2
14	13	21.43	15	2
15	13	28.58	15	3
16	13	28.57	25	1
17	13	28.57	20	2
18	15	21.43	20	2
19	11	28.57	20	1
20	11	28.57	15	2
21	13	35.72	15	2
22	13	28.57	25	3
23	15	35.72	20	2
24	15	28.57	20	1
25	13	28.57	20	2
26	11	21.43	20	2
27	13	35.72	20	3

Note: A is laser power (W), B is the scan speed (mm/s), C is exposure time (ms), and D is the number of passes.

2.2.2 Grey relational approach

This method is employed when different output characteristics need to be unified in a process. The first step in the approach is the normalization of responses. These responses are desired in some particular order as surface roughness is desired to be minimized so that surface finish can be of high quality, engraved depth is desired to be maximized to ensure deep markings and

more legibility of prints, kerf width is desired to be maximized in order for surface ablation can be faster and also material removal rate is needed maximized to ensure faster processing, productivity and time-saving.

Based on the target value, equation (1) is utilized in normalizing the kerf width, engraving depth and material removal rate whereas the surface roughness is normalized using equation (2) (Jailani et al. 2009, Jayaraman and Kumar 2014).

$$x_1(\text{k}) = \frac{x_1{}^q(\text{k}) - \min x_1{}^q(k)}{\max x_1{}^q(\text{k}) - \min x_1{}^q(k)} \tag{1}$$

$$x_1(\text{k}) = \frac{\max x_1{}^q(\text{k}) - x_1{}^q(k)}{\max x_1{}^q(\text{k}) - \min x_1{}^q(k)} \tag{2}$$

where $x_1{}^q(k)$ is the measured value of quality characteristic or response, $\max x_1{}^q(k)$ is the largest or highest value of the quality characteristic and $\min x_1{}^q(k)$ is the smallest or the least value of the quality characteristic.

Subsequently, the deviation of the normalized responses was evaluated with equation (3) (Kazançoğlu et al. 2011, Raza et al. 2014).

$$\Delta_{oi}(\text{k}) = \| x_o(k) - x_i(k) \| \tag{3}$$

where $\Delta_{oi}(\text{k})$ is the difference sequence, which is defined as the absolute value of the difference between $x_o(k)$ and $x_i(k)$. Here, $x_o(k)$ and $x_i(k)$ are the normalized values of a response set

(where $x_o(k)$ represents the highest normalized value and $x_i(k)$. represents a set of normalized values from (i = 0 to i = n).

Afterward, the grey relational coefficients for the responses are then computed using equation (4) (Kazançoğlu et al. 2011, Reddy et al. 2015).

$$\xi_i(\text{k}) = \frac{\Delta_{min} + \psi\Delta_{max}}{\Delta_{oi}(k) + \psi\Delta_{min}} \tag{4}$$

Also, ψ is the identification coefficient, which is usually set within 0 and 1. This implies that $0 < \psi < 1$. Most studies set ψ to be equivalent to 0.5. Also, Δ_{min} is the minimum value in the difference sequence and Δ_{max} is the maximum value in the difference sequence while $\xi_i(k)$ is the grey relational coefficient (Ojo and Taban et al. 2018).

Having obtained the grey relational coefficients of the output characteristics, the grey relational grade is computed with equation (5). The principal component analysis is employed to get the weighting values of each of these responses (Jailani, et al. 2009).

$$Y_i = \frac{1}{n}\sum_{i=1}^{n} \xi_i(\text{k}) \tag{5}$$

Where Y_i is the computed GRG for the ith term, n is the number of responses or quality factor, w_k is the normalized weighting value of quality factor k and $\xi_i(k)$ is the Grey relational coefficient.

Surface distance:2158.37nm
Horizontal distance:2158.37nm   Vertical distance:1.87nm
Angle(degree):-0.05   Roughness Ra:0.12 nm
Height[Red]:7.01nm   Height[Greeb]:5.14nm
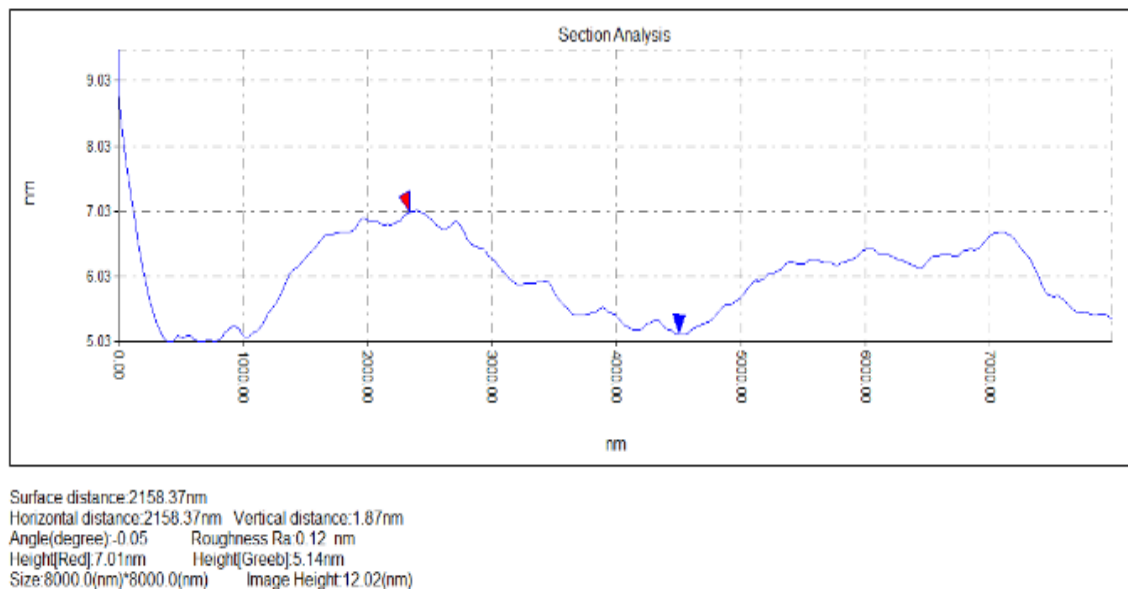Size:8000.0(nm)*8000.0(nm)   Image Height:12.02(nm)

Fig. 6. Imager showing engraving depth section

2.2.3 Principal component analysis

PCA examines variance-covariance among a given set of quality responses. As a result, the contribution of each of the responses/optimally weighted observed variables can be easily evaluated (Shlens 2014). A matrix of the observed responses is required to commence data reduction in PCA. As a result, the grey relational coefficient (GRC) of each of the observed responses is required to formulate a data matrix. If the element of the data matrix is denoted as $Y_i(k)$, then i is set to vary from 1 to m while k is defined to vary from 1 to n as illustrated in equation (6).

$$Y_i(k) = \begin{bmatrix} Y_1(1) & Y_1(2) & Y_1(3) & \dots\dots\dots & Y_1(n) \\ Y_2(1) & Y_2(2) & Y_2(3) & \dots\dots\dots & Y_2(n) \\ Y_3(1) & Y_3(2) & Y_3(3) & \dots\dots\dots & Y_3(n) \\ \vdots & \vdots & \vdots & \vdots\ \vdots\ \vdots & \vdots \\ \vdots & \vdots & \vdots & \vdots\ \vdots\ \vdots & \vdots \\ Y_m(1) & Y_m(2) & Y_m(3) & \dots\dots\dots & Y_m(n) \end{bmatrix} \quad (6)$$

Where $Y_i(k)$ are the responses, n is the number of columns, or the number of responses and m is the number of rows or the number of experiments. As a result, in this BBD–GRA–PCA approach, Y is the Grey relational coefficients of the observed responses (SR, KW, ED, and MRR).

According to (Mehat et al. 2014) and (Fung and Kang 2005) correlation matrix can be expressed as equation (7).

$$R_{kd} = \left[\frac{Cov(Y_i(k), Y_i(l))}{\sigma_{yi}(k)\sigma_{yk}(l)} \right] \quad (7)$$

where k and l vary from 1 to n. Also, the covariance's of sequences $Y_i(k)$ and $Y_i(l)$ are defined as $Y_i(l)$ while the standard deviation of sequences $Y_i(k)$ and $Y_i(l)$ are defined as $\sigma_{yi}(k)$ and $\sigma_{yk}(l)$, respectively. The relationship among eigenvalue, eigenvector and correction matrix are illustrated with equation (8). With this mathematical expression, the values of

unknown's eigenvalues and eigenvectors can be computed:

$$[R - \lambda I]V = 0 \quad (8)$$

where λ is the eigenvalue, I is an identity matrix, V is the eigenvector and R is the correlation matrix.

The principal components are determined using equation (9) (Fung and Kang 2005). Thus, the optimal weighting values of the responses are equivalent to the percentage contributions of the responses.

$$P_{mi} = \sum_{i=1}^{n} y_m(i)v \quad (9)$$

where P_{mi} is the principal component (P_{m1}, P_{m2}, P_{m3}, and P_{m4} are the 1st, 2nd, 3rd, and 4th principal components, respectively).

3. RESULTS AND DISCUSSION

3.1 Experimental Results

The experimental results from lab testing on the engraved stainless-steel samples to investigate its surface roughness, kerf width, engraved depth, and material removal rate were analyzed, and the responses obtained are presented in Table 4. Different parametric combinations yielded unique output characteristics on the selected responses as observed from the Table 4.

3.2 Single Optimization of Responses

The surface roughness is one of the most important output characteristics to look after while performing laser engraving, especially using stainless steel. The engraved surface is desired to have an extremely low surface roughness as far as possible and the effect of input setting such as laser power, exposure time, scan speed (transverse speed) and number of passes are studied.

Table 4. Process parameters and the corresponding output characteristics

No	Process Parameter				Output Characteristics			
	A (W)	B (mm/s)	C (ms)	D	SR (nm)	KW (nm)	ED (nm)	MRR ((nm^3/s) 10^{11})
1	15	28.57	20	3	0.507	1438.94	1.53	1.08
2	13	21.43	25	2	0.256	1313.81	0.86	0.72
3	13	28.57	15	1	0.254	809.41	0.65	1.36
4	13	28.57	20	2	1.11	1884.75	2.93	2.07
5	11	28.57	25	2	0.438	2318.54	0.92	0.74

| No	Process Parameter				Output Characteristics			
	A (W)	B (mm/s)	C (ms)	D	SR (nm)	KW (nm)	ED (nm)	MRR ((nm^3/s) 10^{11})
6	13	35.72	20	1	0.319	1614.89	0.74	1.41
7	13	35.72	25	2	0.38	1552.35	0.74	0.62
8	13	21.43	20	1	0.195	1376.35	0.86	1.03
9	11	28.57	20	3	0.314	3088.81	4.26	3.04
10	13	21.43	20	3	0.278	1474.12	2.13	1.34
11	15	28.57	15	2	0.315	1223.86	1.44	1.53
12	11	35.72	20	2	0.424	1995.93	0.66	0.63
13	15	28.57	25	2	0.339	1888.59	2.33	1.88
14	13	21.43	15	2	0.195	340.17	0.33	0.36
15	13	28.58	15	3	0.337	907.18	1.92	1.36
16	13	28.57	25	1	0.315	1783.05	1.18	1.92
17	13	28.57	20	2	1.06	1884.75	2.88	2.62
18	15	21.43	20	2	0.238	1636.35	1.83	1.73
19	11	28.57	20	1	0.486	1462.21	0.79	1.45
20	11	28.57	15	2	0.34	1035.99	0.75	0.79
21	13	35.72	15	2	1.01	578.71	1.45	1.61
22	13	28.57	25	3	0.398	1880.82	2.45	1.35
23	15	35.72	20	2	0.362	1874.89	1.71	1.63
24	15	28.57	20	1	0.169	2870	4.04	8.04
25	13	28.57	20	2	1.01	1884.75	2.83	2.6
26	11	21.43	20	2	0.299	1757.39	0.78	0.74
27	13	35.72	20	3	0.402	1712.66	2.01	1.26
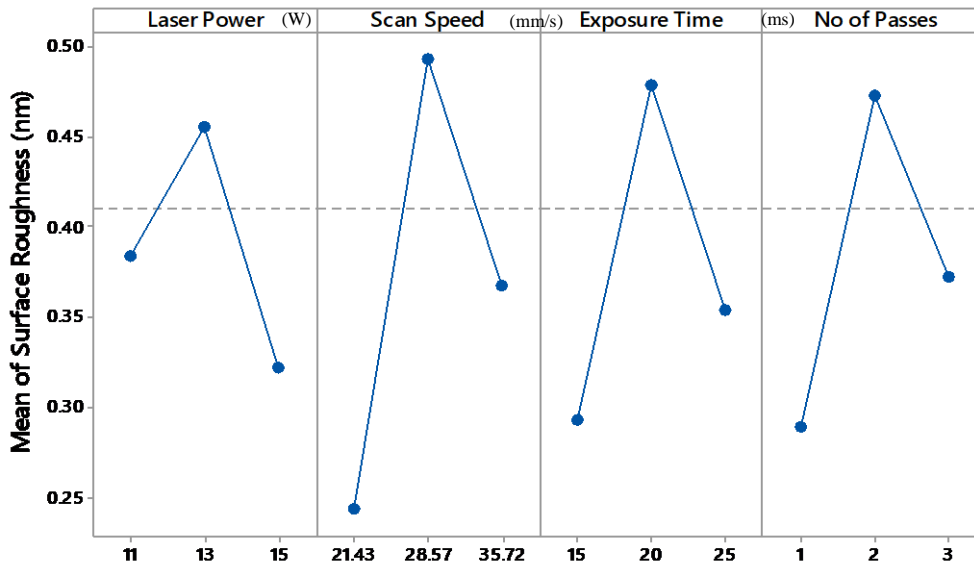
Fig. 7. Main effect plot of surface roughness

The main effect plot as seen in Fig. 7 has shown the interactions between the individual process factors on surface roughness and the best mix to yield the minimal surface response can be deduced from the plot. A combination of (1, -1, -1, -1) yields the best surface roughness for the experiment. The regression equation for predicting surface roughness is presented in equation (10).

Surface Roughness =

$$-25.742 + 2.0358a + 0.4565b + 0.6261c + 0.6588d - 0.08237a^2 - 0.007836b^2 - 0.014900c^2 - 0.36150d^2 - 0.00185ac + 0.06375ad \tag{10}$$

Where a is the laser power, b is the scan speed, c is the exposure time and d is the number of passes.

The contributing effect of laser power, scan speed, exposure time and no of passes on the surface roughness were further investigated with ANOVA where it is observed that there is a linear contribution of 5.56%, a quadratic contribution of 90.01% and a 2-way interaction with contributing effect of 4.13% being the least. The quadratic or square contribution model shows the effect of the square of scan speed with 18.65%, square of exposure time with 23.68% and the square of no of passes having the most significant effect with 43.31%. However, the experiment showed a less significant effect of laser power on surface roughness. This might be a result of the type of laser chosen for this experiment or its capacity which differs from previous experimental conditions.

The kerf width size is desired to be maximized as it determines the rapidity of the surface ablation process. From the analyzed experimental data, it is found that the laser power intensity at the workpiece surface and the exposure time of the laser beam on the surface influences significantly the kerf width size, ANOVA shows the kerf width relationship with all four of the input parameters and their various contributions, the linear model shows a percentage contribution of 32.55%, the quadratic model has 40.58% contribution while the 2-way interaction has the least percentage contribution of 26.75%.

The main effect plot for kerf width in Fig. 8 shows the relationship of laser power, the scan speed, exposure time and the no of passes. The combination to give a maximum kerf width from the main effect plot is (-1, 0, 0, 1) for the input parameters and this combination yields a maximum kerf width of 3088.81 nm. The exposure time has the most significant interaction on the kerf width as a result of the high input energy due to increased interaction time. While optimizing kerf width, a 25.62% interaction was observed between laser power and the number of passes which shows both factors affect the response significantly. The regression equation for determining the kerf width at different combinations of input factors is expressed in equation (11).

Kerf width =
$$-16924 - 867.9a + 440.2b + 1216.8c + 4928d + 73.50a^2 - 6.969b^2 - 22.203c^2 + 22.4d^2 - 15.45ac - 382.21ad - 1.166bc \tag{11}$$

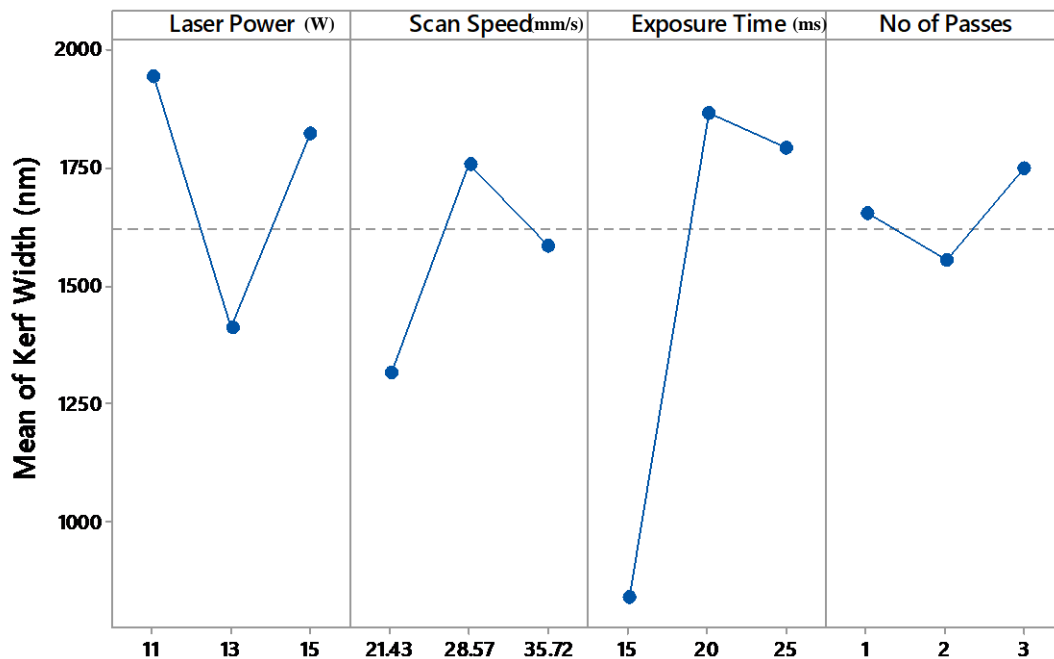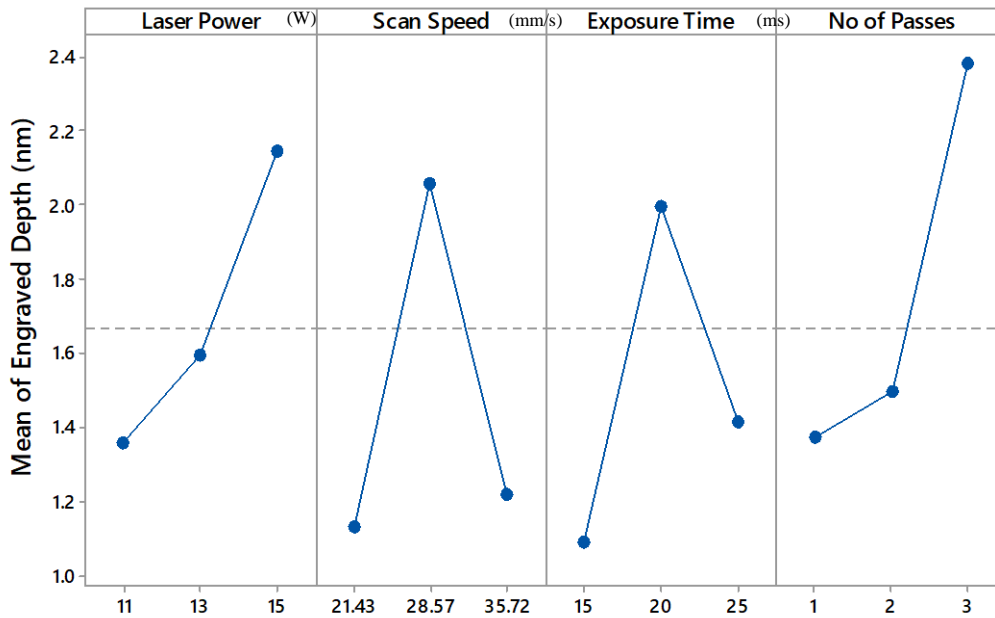Where: a is the laser power, b is the scan speed, c is the burning time and d is the number of passes.

Fig. 8. Main effect plot of kerf width

Fig. 9. Main effect plot of engraved depth

Engraving depth is one of the key output characteristics to look out for as we desired a deep level of engraving on the material surface to ensure clarity of engraving. The ANOVA shows a linear contribution of 18.41%, the quadratic contribution of 41.24% and a 2-way interaction of 33.27%. The main effect plot in Fig. 9 furthermore illustrated the trends of each of the factors and how it affects engraved depth.

The combination to give the best individual response for the engraved depth is (1, 0, 0, 1). The engraving depths are mainly affected by scan speed, laser power and fill density and two of these input parameters adopted for the experiment show a significant effect on engraving depth thus validating the outcome of the experiment. However, the experiment has proven that more passes increase the engraving depth as more interaction occurs between the surface and laser beam due repetitive condition and also a significant interaction of 35.76% exists between the laser power and number of passes. The regression equation for engraving depth is expressed in the equation (12) to obtain desired engraving depth at any combination of the factors.

Engraved depth =
$$-71.8 + 3.44a + 1.515b + 1.770c + 10.76d - 0.0812a^2 - 0.02336b^2 - 0.04310c^2 - 0.135d^2 + 0.0180ac - 0.748ad - 0.00868bc \tag{12}$$

Where: a is the laser power, b is the scan speed, c is the burning time and d is the number of passes.

The material removal rate is the specific amount of ablation that is being removed from a surface per unit time. The focus of this study is to maximize time by ensuring the rate of material removal is higher. As such, lesser time will be needed to perform engraving on a surface and economically, the lesser the time for production, the higher the income. ANOVA shows the Material removal rate has a linear contribution of 17.58%, a quadratic contribution of 30.67% and a 2-ways interaction of achieved of 35.08% on the material removal rate. Laser power and number of passes exhibit a significant interaction of 34.01% on material removal rate.

The main effect plot in Fig. 10 describes the relationship between the material removal rate and how several input parameters influence its response. The combination to give the best MRR is (1, 0, 0, -1). The regression equation for the material removal rate is expressed in equation (13) to obtain the desired response at any combination of the input factors.

$$\begin{aligned}
MRR = {} & -6898102613910 + 229506568688a + 153031639597b + 201072611122c + 1282236514608d - \\
& 44495266a^2 - 2355534377b^2 - 4536510962c^2 + 24246886501d^2 + 16029135ab + 1012267562ac \\
& - 106841906317ad - 937852744bc + 443332501bd - 2807711211cd \hspace{2cm} (13)
\end{aligned}$$

Where: a is the laser power, b is the scan speed, c is the burning time and d is the number of passes.
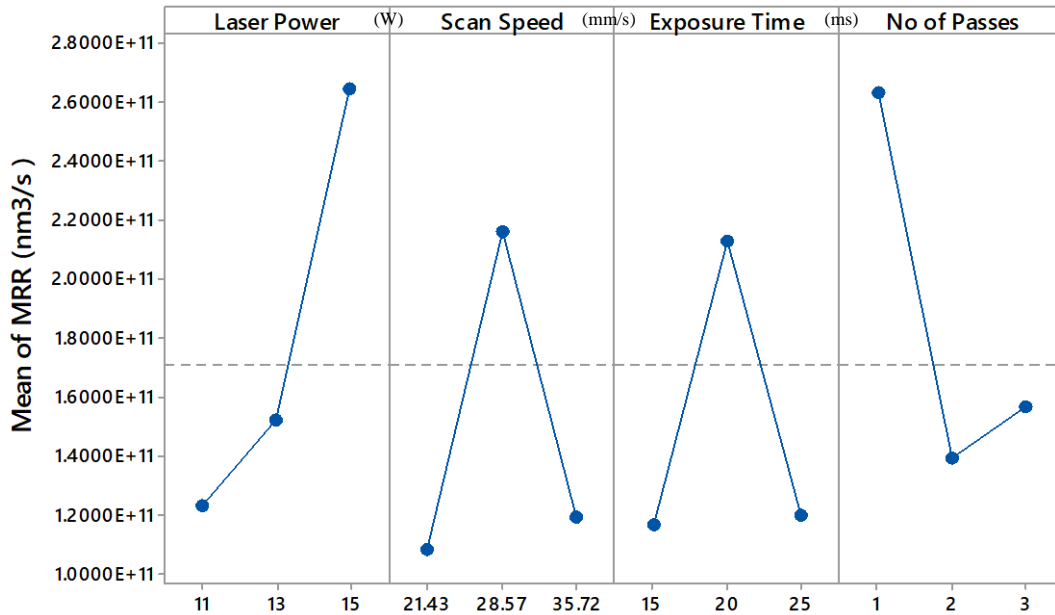

Fig. 10. Main effect plot of material removal rate

Analysis of variance was employed to show the significant effect and interaction plot was also obtained between some of the process factors. It was observed that increment in laser power yields a corresponding increase in material removal rate and engraving depth. Laser power has been shown to have a significant effect on kerf width. However, laser power does not significantly influence surface roughness due to the range of laser power selected (max power 15W laser).

Scan speed shows a significant effect on surface roughness, engraving depth, and material removal rate from the ANOVA. Also, scan speed has shown not to have a significant effect on kerf width.

Exposure time has a significant effect on kerf width. Engraving depth, kerf width and material removal rate. A direct relationship exists between multiple passes and responses such as kerf width and engraving depth. On the other hand, a decrease in material removal rate occurs as the number of passes increases.

3.3 Multi-Objective Optimization

Having obtained the single optimization results, it was observed that the parametric settings to achieve the best of each of the desired target responses are different, thus the need to further harmonize these responses in order to get the optimal process factor that will yield the desirable responses at once. However, the suitability of these chosen responses needs the right set of parametric combinations as single optimization of each response will not necessarily produce the best combination for other response hence it becomes imperative to conduct a multi-objective optimization analysis to determine a unified combination of process parameters, that will be responsible for a low surface roughness, deep engraved depth, wide kerf width and a faster material removal rate on engraved material. Hence grey relational approach with principal component analysis was adopted to obtain the optimum parameters needed to yield the desired target response's combined together.

The responses obtained in Table 4 were normalized according to Eq. (3) and Eq. (4) and the corresponding normalized responses are presented in Table 5.

Consequently, after finding the normalized responses, the next step in the grey relational approach is computing the difference sequence and grey relational coefficient. Eq. (4) and Eq. (5)

was used for the computation respectively presented in Table 6.

Having obtained the grey relational coefficients of the output characteristics, the grey relational grade is computed with equation (5). However, to scientifically obtain the weighting factor for each of the output characteristics, the grey relational coefficient data in Table 5 was subjected to principal component analysis (PCA). For PCA to deliver best results, the grey relational coefficients for the output characteristics must be highly correlated (Ojo and E. Taban 2018, Farayibi and Omiyale 2020). Equation (7) was employed for correlating the grey coefficient and resulting data presented in Table 7 while corresponding eigenvectors were evaluated using equation (8) and obtained eigenvectors tabulated in Table 8.

Equation (9) was used to determine the contribution of the variables of each of the grey relational coefficient also knows as weighting values and its result is reported in Table 9.

The first principal component (F1) contribution as shown in Fig. 11 of the scree plot has the largest cumulative variability and it was used to obtain the grey relational grade.

The obtained weighting values of the responses from the PCA together with the Grey relational coefficient were employed in computing the GRG according to equation (5) and thus, the computed GRGs for the multi-response optimization process are shown in Table 10.

Similarly, the comparison of the multi-response's GRGs with the ideal or reference sequence (unity) is basically used to identify the best parameter combination and to also provide the order of significance of each parameter combination. The largest GRG (closest to unity) is considered to give the best combination of quality responses and process parameters.

Table 5. Normalized responses

Exp. no	Normalized SR	Normalized KW	Normalized ED	Normalized MRR
1	0.6408	0.6002	0.3053	0.0937
2	0.9075	0.6458	0.1349	0.0463
3	0.9097	0.8293	0.0814	0.1304
4	0.0000	0.4381	0.6616	0.3040
5	0.7141	0.2802	0.1501	0.0495
6	0.8406	0.5362	0.1043	0.1372
7	0.7758	0.5590	0.1043	0.0339
8	0.9724	0.6230	0.1349	0.1650
9	0.8459	0.0000	1.0000	0.3493
10	0.8842	0.5875	0.4580	0.1280
11	0.8448	0.6785	0.2824	0.1517
12	0.7295	0.3976	0.0840	0.0351
13	0.8193	0.4367	0.5089	0.1975
14	0.9724	1.0000	0.0000	0.0000
15	0.8215	0.7937	0.4046	0.1296
16	0.8448	0.4751	0.2163	0.2027
17	0.0531	0.4381	0.6489	0.2947
18	0.9272	0.5284	0.3817	0.1785
19	0.6631	0.5918	0.1170	0.1422
20	0.8183	0.7468	0.1069	0.0564
21	0.8406	0.8526	0.2850	0.1622
22	0.7566	0.4395	0.5394	0.1287
23	0.7949	0.4416	0.3511	0.1658
24	1.0000	0.0796	0.9440	1.0000
25	0.1063	0.4381	0.6361	0.2920
26	0.8618	0.4844	0.1145	0.0491
27	0.7524	0.5007	0.4275	0.1165

Table 6. Computed deviation of the normalized S/N values and corresponding grey relational coefficients of the output characteristics

No	Computed Deviation, Δoi(k)				Grey Relational Coefficient			
	SR	KW	ED	MRR	GRC	GRC	GRC	GRC
1	0.3592	0.3998	0.6947	0.9063	0.5819	0.5557	0.4185	0.3555
2	0.0925	0.3542	0.8651	0.9537	0.8439	0.5853	0.3663	0.3439
3	0.0903	0.1707	0.9186	0.8696	0.847	0.7455	0.3525	0.3651
4	1	0.5619	0.3384	0.696	0.3333	0.4708	0.5964	0.418
5	0.2859	0.7198	0.8499	0.9505	0.6362	0.4099	0.3704	0.3447
6	0.1594	0.4638	0.8957	0.8628	0.7583	0.5188	0.3583	0.3669
7	0.2242	0.441	0.8957	0.9661	0.6904	0.5313	0.3583	0.341
8	0.0276	0.377	0.8651	0.835	0.9476	0.5701	0.3663	0.3745
9	0.1541	1	0	0.6507	0.7644	0.3333	1	0.4345
10	0.1158	0.4125	0.542	0.872	0.8119	0.5479	0.4799	0.3644
11	0.1552	0.3215	0.7176	0.8483	0.7632	0.6086	0.4107	0.3708
12	0.2705	0.6024	0.916	0.9649	0.649	0.4536	0.3531	0.3413
13	0.1807	0.5633	0.4911	0.8025	0.7346	0.4702	0.5045	0.3839
14	0.0276	0	1	1	0.9476	1	0.3333	0.3333
15	0.1785	0.2063	0.5954	0.8704	0.7369	0.7079	0.4564	0.3649
16	0.1552	0.5249	0.7837	0.7973	0.7632	0.4878	0.3895	0.3854
17	0.9469	0.5619	0.3511	0.7053	0.3456	0.4708	0.5874	0.4148
18	0.0728	0.4716	0.6183	0.8215	0.8729	0.5146	0.4471	0.3784
19	0.3369	0.4082	0.883	0.8578	0.5975	0.5505	0.3615	0.3682
20	0.1817	0.2532	0.8931	0.9436	0.7334	0.6639	0.3589	0.3464
21	0.1594	0.1474	0.715	0.8378	0.7583	0.7724	0.4115	0.3737
22	0.2434	0.5605	0.4606	0.8713	0.6726	0.4715	0.5205	0.3646
23	0.2051	0.5584	0.6489	0.8342	0.7091	0.4724	0.4352	0.3748
24	0	0.9204	0.056	0	1	0.352	0.8993	1
25	0.8937	0.5619	0.3639	0.708	0.3588	0.4708	0.5788	0.4139
26	0.1382	0.5156	0.8855	0.9509	0.7835	0.4923	0.3609	0.3446
27	0.2476	0.4993	0.5725	0.8835	0.6688	0.5003	0.4662	0.3614

Table 7. Correlation matrix

Variables	GRC SR	GRC KW	GRC ED	GRC MRR
GRC SR	**0.027047**	0.000	-0.002	0.005
GRC KW	0.000	**0.018926**	0.018	0.010
GRC ED	-0.002	0.018	**0.024682**	0.013
GRC MRR	0.005	0.010	0.013	**0.014765**

Table 8. Eigenvectors

	F1	F2	F3	F4
GRC SR	0.021	0.973	-0.206	0.105
GRC KW	0.579	-0.049	-0.499	-0.643
GRC ED	0.688	-0.114	-0.104	0.709
GRC MRR	0.436	0.196	0.836	-0.270

Table 9. Contribution of the variables (%)

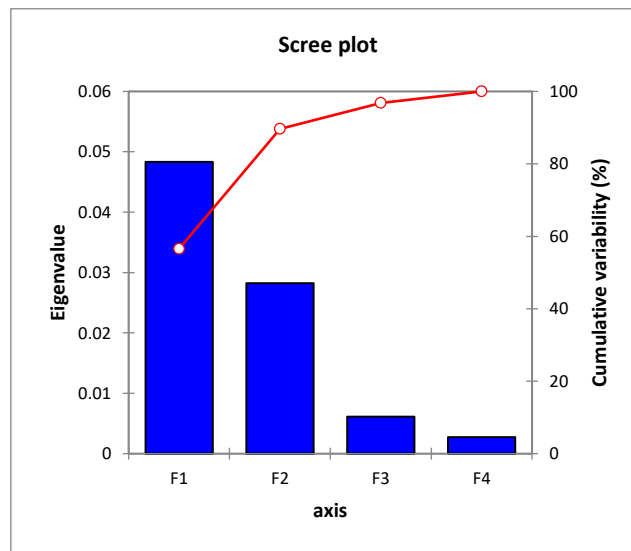|	F1	F2	F3	F4
GRC SR	0.046	94.604	4.237	1.113
GRC KW	33.550	0.236	24.873	41.341
GRC ED	47.351	1.300	1.078	50.272
GRC MRR	19.053	3.861	69.812	7.274

Fig. 11. Scree plot

Table 10. Experimental design mix and their corresponding grey relational grade for the outputs

No	Process Parameter				Grey Relational Grade
	A (W)	B (mm/s)	C (ms)	D	GRG
1	15	28.57	20	3	0.41865
2	13	21.43	25	2	0.38575
3	13	28.57	15	1	0.36304
4	13	28.57	20	2	0.54101
5	11	28.57	25	2	0.45636
6	13	35.72	20	1	0.40177
7	13	35.72	25	2	0.39334
8	13	21.43	20	1	0.39460
9	11	28.57	20	3	0.89215
10	13	21.43	20	3	0.45128
11	15	28.57	15	2	0.40780
12	11	35.72	20	2	0.41941
13	15	28.57	25	2	0.49145
14	13	21.43	15	2	0.33361
15	13	28.58	15	3	0.41565
16	13	28.57	25	1	0.43025
17	13	28.57	20	2	0.53619
18	15	21.43	20	2	0.44731
19	11	28.57	20	1	0.39528
20	11	28.57	15	2	0.37081
21	13	35.72	15	2	0.39043
22	13	28.57	25	3	0.49481
23	15	35.72	20	2	0.45595
24	15	28.57	20	1	0.90624
25	13	28.57	20	2	0.53192
26	11	21.43	20	2	0.40731
27	13	35.72	20	3	0.45755

However, the influence of laser engraving parameters on the engraved surfaces is examined via analysis of variance as shown in Table 11.

Table 11. Analysis of variance for GRG

Source	DF	Seq SS	Contribution (%))	Adj SS	Adj MS	F-Value
Model	14	0.433342	90.94	0.433342	0.030953	8.60
Linear	4	0.019892	4.17	0.151889	0.037972	10.55
Laser Power	1	0.002886	0.61	0.000180	0.000180	0.05
Scan Speed	1	0.000802	0.17	0.031348	0.031348	8.71
Exposure Time	1	0.011446	2.40	0.032628	0.032628	9.07
No of Passes	1	0.004757	1.00	0.104073	0.104073	28.92
Square	4	0.170512	35.78	0.170512	0.042628	11.85
Laser Power*Laser Power	1	0.033589	7.05	0.005763	0.005763	1.60
Scan Speed*Scan Speed	1	0.049457	10.38	0.062712	0.062712	17.43
Exposure Time*Exposure Time	1	0.083596	17.54	0.063431	0.063431	17.63
No of Passes*No of Passes	1	0.003871	0.81	0.003871	0.003871	1.08
2-Way Interaction	6	0.242938	50.98	0.242938	0.040490	11.25
Laser Power*No of Passes	1	0.242291	50.85	0.242291	0.242291	67.33
Scan Speed*Exposure Time	1	0.000607	0.13	0.000607	0.000607	0.17
Error	12	0.043182	9.06	0.043182	0.003598	
Lack-of-Fit	10	0.043140	9.05	0.043140	0.004314	208.31
Pure Error	2	0.000041		0.000041	0.000021	
Total	26	0.476524	100.00			

S   0.0599874   R-Sq   90.94%

The optimal combination of the process parameters (laser power, scan speed, exposure time and no of passes) that produces the best combination of the surface quality characteristics is evaluated through the consideration of GRG. Based on the high grey relational grade obtained which is close to unity, we can conveniently ascertain that experiment 24 having the largest GRG yields the best responses as targeted for this research. The optimal combination of the process parameters obtained therefore are (1, 0, 0, -1) which implies 15 W laser power, 28.57 mm/s scan speed, exposure time of 20 ms and (1) no of pass.

4. CONCLUSION

This study developed and tested a 15W laser engraving machine on AISI 304 stainless steel to explore the relationship between selected process parameters and various responses. A multi-objective optimization approach combining Principal Component Analysis (PCA) and Grey Relational Analysis (GRA) was used to identify the optimal set of parameters for achieving low surface roughness, deep engraving depth, wide kerf width, and fast material removal rate. The following conclusions were drawn:

   i.   In the single response optimization of the laser engraved surfaces of stainless steel AISI 304, it was observed that employing a laser power of 15 W, scanning speed of 21.43 mm/s, exposure time of 15 ms, and 1 pass resulted in the least surface roughness of 0.1775 nm. A combination of 11 W laser power, 28.57 mm/s speed, 20 ms exposure time, 3 passes yielded the best kerf width of 3088.81 nm. Maximum groove depth of 1.822 nm was achieved at 15 W laser power, 28.57 mm/s speed, 20 ms exposure time and 3 laser passes. the maximum material removal rate of 8.04 (10^{11}) nm^3/s was achieved with 15 W, 28.57 mm/s, 20 ms, and 1 laser pass.

   ii.   In the multi-objective optimization, grey relational grade analysis revealed that the optimal combination for achieving the best balance across all responses was 15 W laser power, 28.57 mm/s scanning speed, 20 ms exposure time, and 1 pass.

DISCLAIMER (ARTIFICIAL INTELLIGENCE)

Author(s) hereby declare that NO generative AI technologies such as Large Language Models (ChatGPT, COPILOT, etc) and text-to-image generators have been used during writing or editing of this manuscript.

COMPETING INTERESTS

Authors have declared that no competing interests exist.

REFERENCES

Ahmed, N., Darwish, S., & Alahmari, A. M. (2016). Laser ablation and laser-hybrid ablation processes: A review. *Materials and Manufacturing Processes, 31*(9), 1121–1142. https://doi.org/10.1080/10426914.2015.1048359

Arnold, N. (2002). Dry laser cleaning of particles by nanosecond pulses: Theory. In *Laser Cleaning* (pp. 51–102). World Scientific. https://doi.org/10.1142/9789812777515_0002

Brousseau, E. B., Dimov, S. S., & Pham, D. T. (2010). Some recent advances in multi-material micro- and nano-manufacturing. *International Journal of Advanced Manufacturing Technology, 47*(1), 161–180. https://doi.org/10.1007/s00170-009-2214-5

Brown, M. S., & Arnold, C. B. (2010). Fundamentals of laser-material interaction and application to multiscale surface modification. In K. Sugioka, M. Meunier, & A. Piqué (Eds.), *Laser precision microfabrication* (pp. 91–120). Springer. https://doi.org/10.1007/978-3-642-10523-4_4

Campanelli, S. L., Ludovico, A. D., Bonserio, C., Cavalluzzi, P., & Cinquepalmi, M. (2007). Experimental analysis of the laser milling process parameters. *Journal of Materials Processing Technology, 191*(1), 220–223. https://doi.org/10.1016/j.jmatprotec.2007.03.005

Farayibi, P. K., & Omiyale, B. O. (2020). Mechanical behaviour of polylactic acid parts fabricated via material extrusion process: A Taguchi-grey relational analysis approach. *International Journal of Engineering Research in Africa, 46*, 32–44. https://doi.org/10.4028/www.scientific.net/JERA.46.32

Fung, C.-P., & Kang, P.-C. (2005). Multi-response optimization in friction properties of PBT composites using Taguchi method and principle component analysis. *Journal*

of Materials Processing Technology, 170(3), 602–610. https://doi.org/10.1016/j.jmatprotec.2005.06.040

González, M., Ramos-Grez, J. A., Jeria, I., Guerra, C., Solis, R., Carvajal, L., & Solis, R. (2023). Effects of laser surface modification on stainless steel 316L thin annular discs under radial and cartesian scans. *Optics & Laser Technology, 157*, 108617. https://doi.org/10.1016/j.optlastec.2022.108617

Haron, M. N. F. B., & Romlay, F. R. B. M. (2019). Parametric study of laser engraving process of AISI 304 stainless steel by utilizing fiber laser system. *IOP Conference Series: Materials Science and Engineering, 469*, 012124. https://doi.org/10.1088/1757-899X/469/1/012124

Hribar, L., Gregorčič, P., Senegačnik, M., & Jezeršek, M. (2022). The influence of the processing parameters on the laser-ablation of stainless steel and brass during the engraving by nanosecond fiber laser. *Nanomaterials, 12*(2), 232. https://doi.org/10.3390/nano12020232

Hubeatir, K. A. (2018). A review: Effect of different laser types on material engraving process. Retrieved October 1, 2022, from https://www.academia.edu/67384586/A_Review_Effect_of_Different_Laser_Types_on_Material_EngravingProcess

Jailani, H. S., Rajadurai, A., Mohan, B., Kumar, A. S., & Sornakumar, T. (2009). Multi-response optimisation of sintering parameters of Al–Si alloy/fly ash composite using Taguchi method and grey relational analysis. *International Journal of Advanced Manufacturing Technology, 45*(3), 362. https://doi.org/10.1007/s00170-009-1973-3

Jayaraman, P., & Kumar, L. M. (2014). Multi-response optimization of machining parameters of turning AA6063 T6 aluminium alloy using grey relational analysis in Taguchi method. *Procedia Engineering, 97*, 100–109. https://doi.org/10.1016/j.proeng.2014.12.242

Kazançoğlu, Y., Esme, U., Bayramoglu, M., Guven, O., & Özgün, S. (2011). Multi-objective optimization of the cutting forces in turning operations using the grey-based Taguchi method. *Materials Technology, 45*, 105–110.

Knowles, M. R. H., Rutterford, G., Karnakis, D., & Ferguson, A. (2007). Micro-machining of metals, ceramics and polymers using nanosecond lasers. *International Journal of Advanced Manufacturing Technology, 33*(1), 95–102. https://doi.org/10.1007/s00170-007-0967-2

Mehat, N., Kamaruddin, S., & Othman, A. (2014). Hybrid integration of Taguchi parametric design, grey relational analysis, and principal component analysis optimization for plastic gear production. *Chinese Journal of Engineering, 2014*, 1–11. https://doi.org/10.1155/2014/351206

Mladenovič, V., Panjan, P., Paskvale, S., Çalışkan, H., Poljanšek, N., & Cekada, M. (2016). Investigation of the laser engraving of AISI 304 stainless steel using a response-surface methodology. *Tehnički Vjesnik - Technical Gazette, 23*, 265–271. https://doi.org/10.17559/TV-20150504150446

Ojo, O. O., & Taban, E. (2018). Hybrid multi-response optimization of friction stir spot welds: Failure load, effective bonded size, and flash volume as responses. *Sādhanā, 43*(6), 98. https://doi.org/10.1007/s12046-018-0882-2

Patel, D., & Patel, D. (2014). Parametric optimization of laser engraving process for different material using grey relational technique- A review. Retrieved October 1, 2022, from https://www.semanticscholar.org/paper/A-Review-on-Laser-Engraving-Process-for-Different-Patel-Chaudhary/6a90c3c0cd68d55fbdde5b3d4e6d8632dd30bbe5

Raza, Z. A., Ahmad, N., & Kamal, S. (2014). Multi-response optimization of rhamnolipid production using grey rational analysis in Taguchi method. *Biotechnology Reports, 3*, 86–94. https://doi.org/10.1016/j.btre.2014.06.007

Reddy, V. C., Deepthi, N., & Jayakrishna, N. (2015). Multiple response optimization of wire EDM on Aluminium HE30 by using grey relational analysis. *Materials Today Proceedings, 2*(4), 2548–2554. https://doi.org/10.1016/j.matpr.2015.07.201

Roy, A., Kumar, N., Das, S., & Bandyopadhyay, A. (2018). Optimization of pulsed Nd:YVO4 laser marking of AISI 304 stainless steel using response surface methodology. *Materials Today Proceedings, 5*(2, Part 1), 5244–5253. https://doi.org/10.1016/j.matpr.2017.12.107

Saklakoglu, I. E., & Kasman, S. (2011). Investigation of micro-milling process parameters for surface roughness and milling depth. *International Journal of Advanced Manufacturing Technology, 54*(5), 567–578. https://doi.org/10.1007/s00170-010-2953-3

Sheu, D. D. (2000). A laser marking system for flexible circuit identification. *Journal of Manufacturing Systems, 19*(3), 202–212. https://doi.org/10.1016/S0278-6125(00)80012-6

Shlens, J. (2014). A tutorial on principal component analysis. *arXiv*. https://doi.org/10.48550/arXiv.1404.1100

Stavropoulos, P., Efthymiou, K., & Chryssolouris, G. (2012). Investigation of the material removal efficiency during femtosecond laser machining. *Procedia CIRP, 3*, 471–476. https://doi.org/10.1016/j.procir.2012.07.081

Sugar, P., Mikolas, J., & Sugarova, J. (2013). Experimental study of Nd:YAG laser machining of Cr-Ni austenitic stainless steel. *Tehnički Vjesnik - Technical Gazette, 20*(4), 577–581.

Zeng, Z., Cheng, W., Li, X., & Sun, Y. (2024). High strength-ductility synergy in an austenitic stainless steel by laser processing. *Materials Today Communications, 41*, 110329. https://doi.org/10.1016/j.mtcomm.2024.110329

Peer-review history:
The peer review history for this paper can be accessed here:
https://www.sdiarticle5.com/review-history/127113